Behavior of FRP Strengthened RC Beams under Static and Impact Loads

Thong M. Pham[1] and Hong Hao[2]

Abstract

This study investigates the behavior of fiber reinforced polymer (FRP) strengthened reinforced concrete (RC) beams under static and impact loads. The experimental program includes six beams tested in static loads and seven beams tested against impact loads. Longitudinal FRP strips and FRP U-wraps were used to strengthen these beams. The section of four beams was modified to have a curved-soffit in order to reduce the stress concentration of FRP U-wraps and provide confinement effect on longitudinal FRP strips. The experimental results showed that the proposed modification significantly increased the beam capacities as compared to their rectangular counterparts strengthened with the same amount of FRP material. In addition, this paper also provides explanations and discussions on the phenomenon of shifting of the flexure failure mode under static loads to the shear-flexure failure mode under impact loads of all the beams tested in the study, as well as the proper interpretations of the measured impact forces in the tests. From the experimental results, it is recommended that the impact force and inertial force at the very early stage of an impact event should be used to design the impact resistance.

Keywords: Fiber Reinforced Polymer (FRP); Impact loading; Impact resistance; Strengthening; Retrofitting.

[1] Research Fellow, Center for Infrastructural Monitoring and Protection, School of Civil and Mechanical Engineering, Curtin University, Kent Street, Bentley, WA 6102, Australia (Corresponding author). Email: thong.pham@curtin.edu.au

[2] John Curtin Distinguished Professor, Center for Infrastructural Monitoring and Protection, School of Civil and Mechanical Engineering, Curtin University, Kent Street, Bentley, WA 6102, Australia. Email: hong.hao@curtin.edu.au

1 Introduction

Recent global terrorism activities and threats imposed noticeable danger to the public infrastructure, and thus effective impact resistance design of structures have been increasingly attracting the research society. Reinforced concrete structures may be subjected to impact loads during its service life, for example rock fall, vehicle collision, ship impact, and accidently dropping heavy objects on structures. Fiber reinforced polymer (FRP) has been commonly used in the field of civil engineering for a few decades. This material can be utilized to improve the impact resistance of structures. It has been used in strengthening or retrofitting existing structures, or building new structures ranging from beams, slabs, columns, to walls [1, 2]. Among those types of structures, reinforced concrete (RC) beams can be strengthened with FRP regarding to shear failure or flexural failure to resist impact loads. The structural behaviors of RC beams against impact loads have been studied and presented in the literature. Unfortunately, structural behaviors of RC beams strengthened with FRP against impact loading are limited to a few qualitative studies [3-6].

Erki and Meier [5] conducted tests on 8-m-long RC beams (Beams BF1 and BF2) strengthened for flexure resistance. The strain rate of FRP during the tests varied from an average of 0.7 s^{-1} (strain/second) to a maximum of over 0.84 s^{-1}. Debonding of the laminate was observed as the primary failure mode of the two beams tested. Since it is difficult to predict the progress of the failure of FRP strengthened RC beams in the test, the first occurrence of the debonding or the rupture of FRP were not determined. Tang and Saadatmanesh [6] tested five RC beams under drop-weight tests. Multiple drops up to 30 were conducted in the study. The authors mentioned that because the impact loading would cause vibration, the top and bottom faces of the beams would experience cyclic tensile and compressive stresses. FRP was bonded to two sides of the beams. During the testing, flexural

cracks first occurred on the bottom face of concrete and propagated upward to the level of the neutral plane. With progressively increasing the impact load, diagonal shear cracks were observed. These cracks extended quickly to the interface of concrete and laminate at the top and bottom surface and then propagated along the interface. These beams finally failed in shear. The debonding strain of FRP was about 4,000 με (micro strain) with the strain rate about 1.4 s^{-1}. Tang and Saadatmanesh [4] further reported experimental tests of 27 concrete beams under impact loading. A total of four types of cracks were observed and flexural cracks first occurred on the bottom face of concrete and then propagated upward to the level of the neutral plane. When the number of impacts or the height of a drop increased, these cracks extended to the interface between the FRP and the concrete. Most of the tested beams failed owing to shear cracks. Experimental results showed that using stiffer FRP can enhance capacities of RC beams under impact loading. Pham and Hao [7] investigated the impact behavior of FRP-strengthened RC beams without stirrups. The authors have conducted drop-weight tests on thirteen beams which were strengthened in shear by different wrapping schemes. Experimental results from that study have shown that the FRP contribution to shear strength can be estimated by the procedure recommended by ACI 440.2R-08 [8] with reasonable accuracy. However, the debonding strain of FRP under impact loads is slightly lower than that under quasi-static loads. Accordingly, actual debonding strains of FRP were recommended for impact loads to achieve better estimations.

The above studies provided observations of failure modes of FRP strengthened RC beams, but have not quantitatively examined the structural behavior of RC beams against impact loading. Time histories of FRP strips along a RC beams have not been available in the literature so that they are examined and discussed. This study aims to study the response of RC beams which are flexurally strengthened with FRP under drop-weight tests. An alternative technique for strengthening RC beams against both static and impact loads are introduced and its excellent

performance was validated against the conventional strengthening technique. By using approximately the same amount of materials, the modified beams eliminated the stress concentration at the FRP U-wraps and provided confining pressure on the longitudinal FRP strip thus enhanced their capacities under both static and impact loads. The main objectives are to study: (1) failure modes and crack patterns of the tested specimens, (2) the dynamic response of the beams and the relations between the measured impact loads, reaction forces and inertial forces, and (3) the effectiveness of a new strengthening method. This study first describes the specimens' design the setup of static and impact tests. The experimental results of the static tests are then presented to demonstrate the efficiency of the proposed strengthening technique. The impact resistance of the modified beams is then compared to that of the conventional strengthening technique to confirm its efficiency. Finally, the dynamic response and time delay of the tested beams are investigated and discussed to provide further understanding of the impact behavior.

2 Strengthening schemes and FRP debonding

RC beams have been successfully strengthened with longitudinal FRP to increase their flexural resistance in quasi-static tests. In such cases, the soffits of beams were bonded with a number of longitudinal FRP strips. However, the effectiveness of this conventional strengthening technique is limited by the debonding of the longitudinal FRP strips. There are many causes leading to the debonding of longitudinal FRP strips as explained in the study by Smith and Teng [9]. The most commonly reported debonding failure occurs at or near the FRP plate ends. This failure is due to high interfacial shear and normal stress [9]. In addition, the debonding becomes more critical as FRP strengthened RC beams are subjected to impact loading. The debonding of FRP has been observed in most of the existing studies about RC beams flexurally strengthened with FRP against impact loading as presented previously.

93 Hamed and Rabinovitch [10] conducted an analytical study about RC beams strengthened by
94 FRP under impulsive loads and found that the peeling stress developed at the edges of the
95 FRP, this phenomenon is similar to that in the static aspect.

96 In addition, the bonding between FRP and concrete in impact tests may be very different from
97 that in static tests. Generally, impact loading is an extremely severe loading condition
98 characterized by a force of great intensity within a short period of time. The behavior of
99 structures under impact loading may consist of two response phases. They are the local
100 response due to the stress wave that is generated at the loading point immediately upon
101 impacting and lasting a very short period of time after the impact and the overall response
102 consisting of the force and free vibration effect with the elastic-plastic deformation which
103 lasts a relatively longer period of time after the impact event. It is worth noting that the
104 overall response is predominantly governed by the loading rate effect and the dynamic
105 behavior of the structural member [11]. The two phases may cause double-impact on the
106 bonding which may lead to a reduction of the bond strength of FRP.

107 In order to mitigate the debonding failure of FRP, transverse FRP strips are bonded to three
108 sides of the beams, namely FRP U-wraps. The use of normal FRP U-wraps cannot generate
109 force to against the peeling stress in the adhesive as shown in Fig. 1, i.e., the tensile force in
110 FRP does not contribute to resist the peeling stress (σ) in the FRP U-wraps in the case of
111 normal rectangular beams. The peeling stress is thus resisted by the tensile stress of the
112 adhesive or concrete near the surface. On the contrary, if the beam soffit is modified to
113 become an arc with a radius r, the FRP U-wraps can generate confining stresses which help to
114 prevent the debonding of longitudinal FRP strips as shown in Fig. 1. In such cases, the
115 peeling stress is resisted by the sum of the tensile stress in adhesive and the confining stress
116 from the FRP U-wraps. The confining stress can be estimated as follows [12]:

$$\sigma = \frac{p}{r} \quad (1)$$

where σ is the confining stress in adhesive, P is the force in the FRP U-wrap, and r is the radius of the beam soffit.

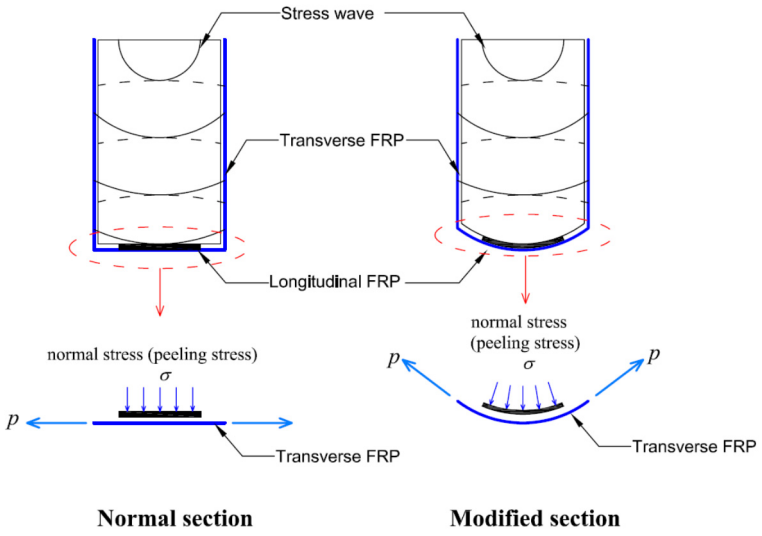

Figure 1. Debonding analysis of FRP under impact loads

3 Experimental program

3.1 Test matrix and material properties

There are two beam groups with different the loading conditions and sections, namely rectangular section and modified section. The beams with a modified section were cast in a special formwork including a rectangular steel formwork and curved polystyrene foam formwork. These beams were designed to fail in flexure so that their static shear capacity is about four times of their static flexural capacity (Table 1). For easier reference, the notation of the beams consists of three parts: The first part is N- and M- that states the shape of the section (**N**ormal rectangular and **M**odified section). The second part indicates the wrapping arrangement in which L is for the number of FRP layers of the longitudinal strip while T stands for the number of transverse strips in half of a beam. For instance, L2T7 means this beam was bonded with two layers of the longitudinal FRP strip and seven one-layer FRP U-

wraps on the half beam. It is noted that the longitudinal FRP strip was bonded before the FRP U-wraps. The third part is to distinguish static loads and impact loads in which A and B are for static and impact, respectively.

It is noted that these beams belong to slender beam group as defined by MacGregor [13] with the shear span ratio (a/d) 4.52 in which a stands for the shear span and d is an effective depth of the beam. The dimensions of the rectangular beams were 150 mm in width, 250 mm in height, and 2200 mm in length. The modified section beams had the same length as the rectangular beams but the section was modified at the soffit which is an arc with a radius of 125 mm. The soffit of the beams was modified in order to postpone the premature debonding of the longitudinal FRP strips and reduce stress concentration of FRP U-wraps. The details of the reinforcement are illustrated in Fig. 2. The nominal tensile strength of deformed bars and plain bars were 500 MPa and 250 MPa, respectively. The ready-mixed concrete used to cast these beams had the compressive strength of 46 MPa at 28-day age.

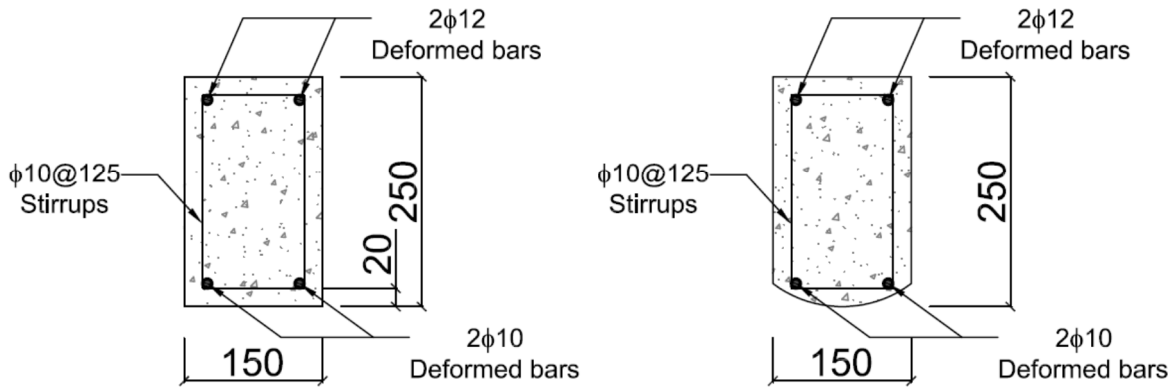

Figure 2. Details of reinforcement

The beams were bonded with a number of FRP layers onto the beam soffit. In order to delay the debonding of FRP, FRP U-wraps were bonded vertically onto three sides of the beams as shown in Fig. 3. FRP was bonded to the substrate of concrete by epoxy resin which has a tensile strength of 54 MPa, tensile modulus of 2.8 GPa, and 3.4% tensile elongation [14]. The

153 adhesive used was a mixture of epoxy resin and hardener at 5:1 ratio. The FRP was the same
154 type and supplier with the one used in a number of studies [15, 16]. The CFRP used was 75
155 mm in width with a unidirectional fiber density of 340 g/m^2. The nominal thickness of FRP
156 was 0.45 mm and the tensile strength was 1548 MPa. The average strain at the maximum
157 tensile force and the average elastic modulus were 1.74% and 89 GPa, respectively, as based
158 on ASTM D3039 [17].

159 Prior to bonding FRP to the beams, careful surface preparation was carried out to remove
160 weak concrete. The concrete surface was roughened by using a pneumatic needle gun (or
161 needle scaler). The concrete surface was blown by an air gun to ensure all dust and weak
162 concrete were removed. The concrete surface was then cleaned by acetone. A primer was
163 applied to the concrete surface before bonding with FRP. The epoxy curing time was
164 maintained at least three days before testing as based on recommendation from the supplier.

165 ***3.2 Strain measurement***

166 A number of strain gauges were bonded to the soffit of the beams to monitor the longitudinal
167 strains with three objectives: (1) obtain the impact load versus FRP strain curves, (2) the
168 distribution of FRP strain along the beams, and (3) the FRP strain at failure in which rupture
169 or debonding of FRP could be expected. These strain gauges were placed at a spacing of 150
170 mm from one end of the beams to the midspan point as shown in Fig. 3. Two strain gauges
171 were also fixed on the side of each FRP U-wrap to monitor the FRP strain during the impact
172 events.
173

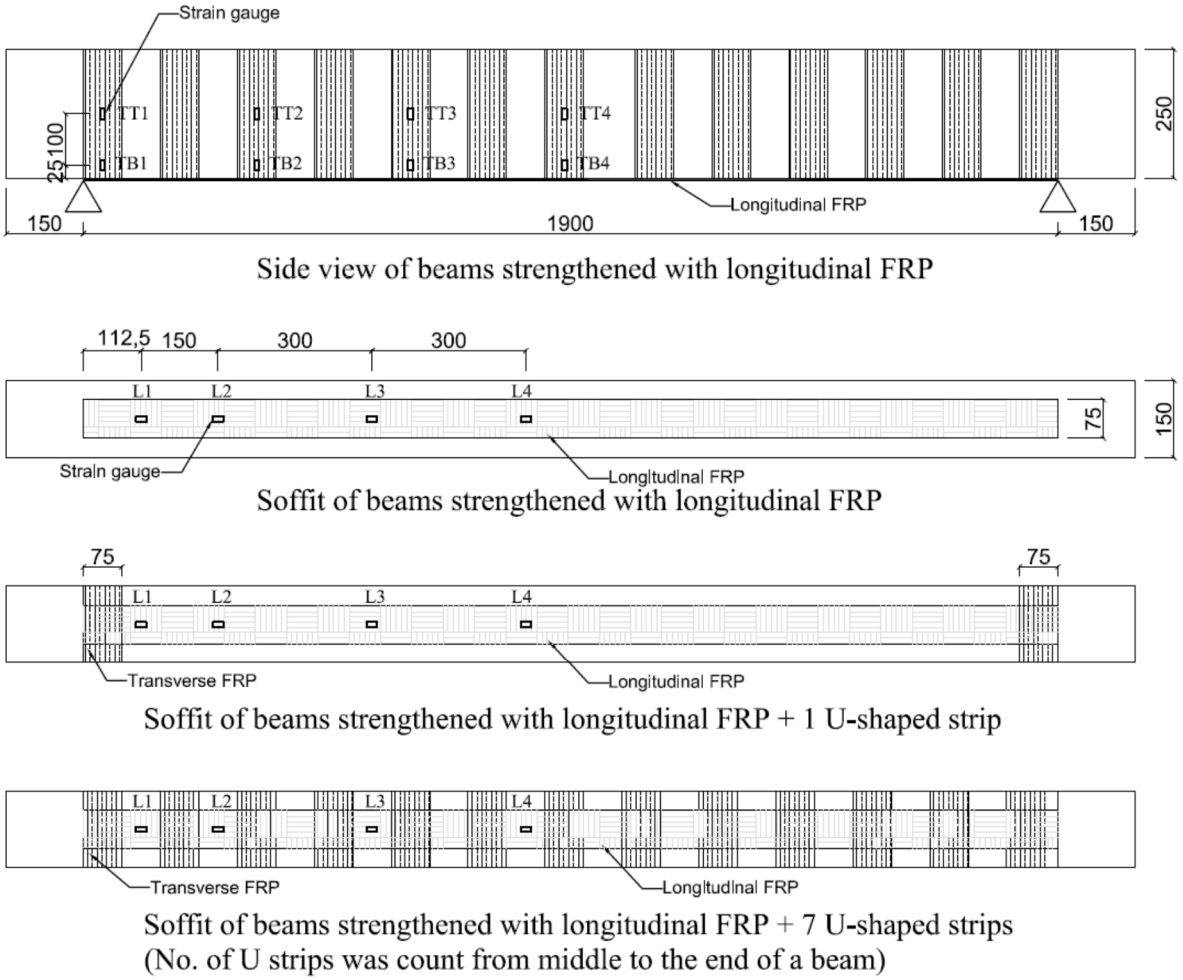

Figure 3. Configuration of strengthening technique

3.3 Testing Procedure

The static tests involved testing six beams and measuring their responses to a monotonically increasing load. The beams were simply supported in a three point loading configuration using a roller and pin, creating an effective span of 1900 mm. The beams were tested using a hydraulic jack with a loading rate at 1 mm/min. The deflections of the beams were measured at different positions by linear variable differential transformers (LVDT).

Drop-weight impact tests were conducted by dropping a weight from a certain height onto the midspan of the beams using the impact test apparatus, as detailed in the study by Pham and Hao [7]. The weight was made of a solid steel cylinder, weighing 203.5 kg. The boundary

condition was carefully designed for center-point flexural impact tests of the simply supported beams as shown in Fig. 4. Two load cells were respectively fixed onto the strong floor and the beam at one end of the beams, as shown in the study by Pham and Hao [7], to be able to measure both positive and negative reaction forces (Fig. 4). A pin and a steel roller were placed on the supports to produce an effective span of 1900 mm. A high-speed camera which was set to capture 5000 frames per second was used to monitor the failure processes. The data acquisition system controlled by a computer was used to record forces from the load cells and strain gauges. The data acquisition system recorded data at the frequency of 50 kHz.

4 Experimental results of static tests

4.1 Failure modes

All beams tested under quasi-static loads failed under the flexure mode since they were designed to have relatively large shear resistance. The shear resistance of these beams is 3.42 – 4.08 times higher than their flexural resistance. Vertical cracks appeared at the midspan of beams when the applied load reached about 18 – 20 kN. These cracks were observed for all beams including the reference beam and the strengthened beams as shown in Fig. 5. As conventional RC beams failing in flexure, new vertical cracks were observed at positions closer to the supports. The widths of these cracks opened and their lengths developed from the soffit of the beams to the top. For the strengthened beams (NL1A, NL2T1A, ML2T1A, and NL2T7A), when the applied load was substantial, the longitudinal FRP strip initially debonded at the midspan and debonding extended to the beam ends. The longitudinal FRP strip still carried tension stress as evidenced by the increasing in longitudinal strain, which will be discussed in the later part in this paper. Accordingly, the tension force in the longitudinal FRP strip horizontally pulled the vertical FRP U-wraps and caused the shear stress in the FRP U-wraps. When the FRP U-wraps ruptured, the beam failed due to

completely debonding of the longitudinal FRP strip as shown in Figs. 6a-d. Interestingly, the FRP U-wraps of Beams ML2T7A did not rupture while rupture of the longitudinal FRP strip caused the failure of this beam (Fig. 6e).

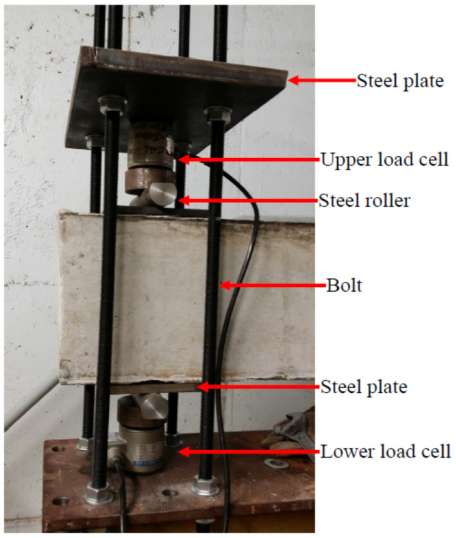

Figure 4. Load cells for positive and negative reactions

4.2 Load-displacement curves

The load – displacement curves of the reference beam and rectangular beams are presented in Fig. 7. At the early stage of loading, the slope of the curves of these beams was almost the same, which means that the contribution of the FRP strip had not been activated yet. When the applied load was greater than 50 kN, the applied load of strengthened beams still increased while the load of the reference beam remained unchanged and decreased afterward. Some discontinuing points observed in the load – displacement curves of the strengthened beams were caused by debonding of the longitudinal FRP strip at the midspan. After FRP debonding stresses in these beams were redistributed and the applied load continued increasing while the debonding of the longitudinal FRP strips extended to positions closer to the supports. The experimental results of these beams are presented in Table 2. When FRP rupture occurred, the applied loads of the strengthened beams dropped to the corresponding

value of the reference beam as shown in Fig. 7. The maximum displacement of these beams summarized in Table 2 indicates the displacement at the maximum load. After the FRP strip ruptured, these beams still could resist a load of the same level as the corresponding load of the reference beam at the same displacement. The capacity of Beam NL1A increased up to 14% while Beams NL2T1A and NL2T2A enhanced by 8 and 20%, respectively as compared to the reference beam. It can be seen that using 2 FRP U-wraps at the ends of the longitudinal strip increases the capacity of the beams. The FRP U-wraps helped to stop debonding of the longitudinal FRP strip. Especially, the capacity of Beam NL2T7A enhanced by up to 59%, in which the longitudinal FRP strip debonded at the load of 66 kN but the FRP U-wraps prevented the propagation of the debonding. As a result, the capacity of Beam NL2T7A increased significantly until all FRP U-wraps ruptured.

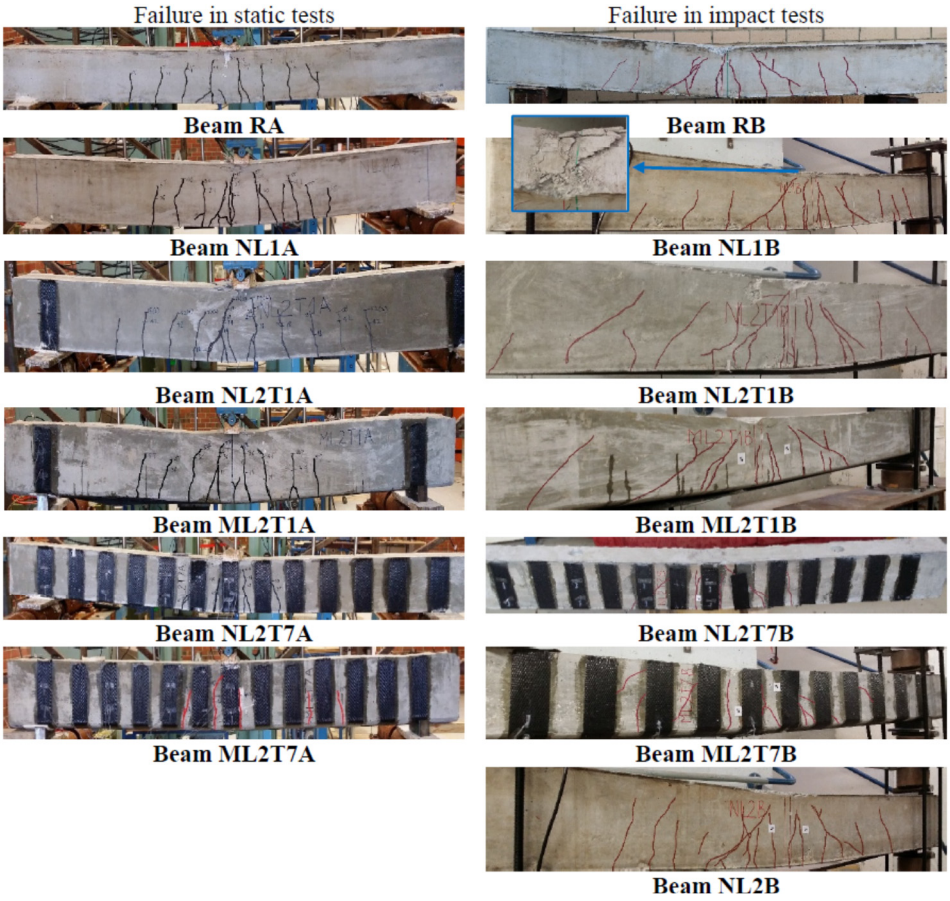

Figure 5. Failure modes of tested beams

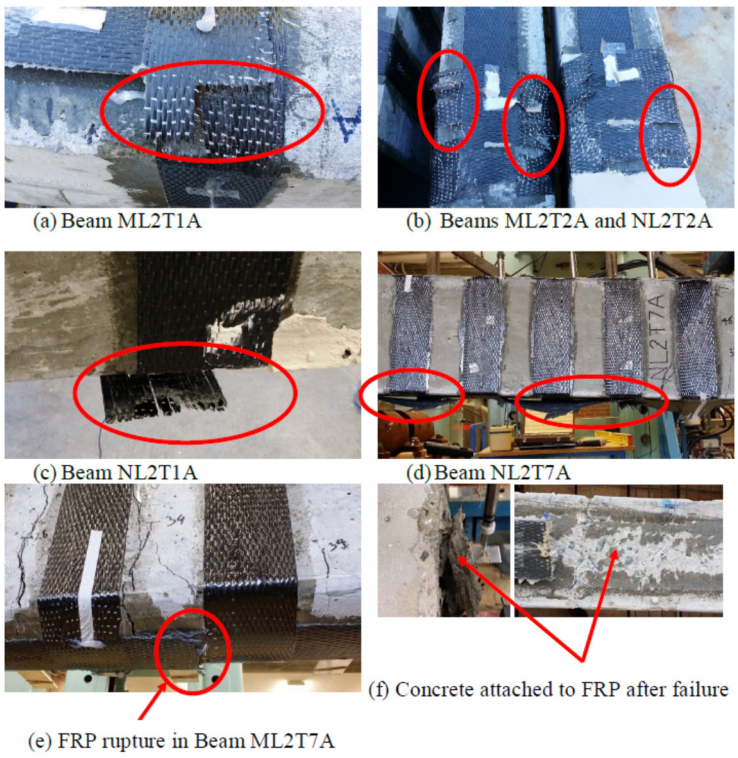

239

240 Figure 6. Ruptures of FRP U-wraps

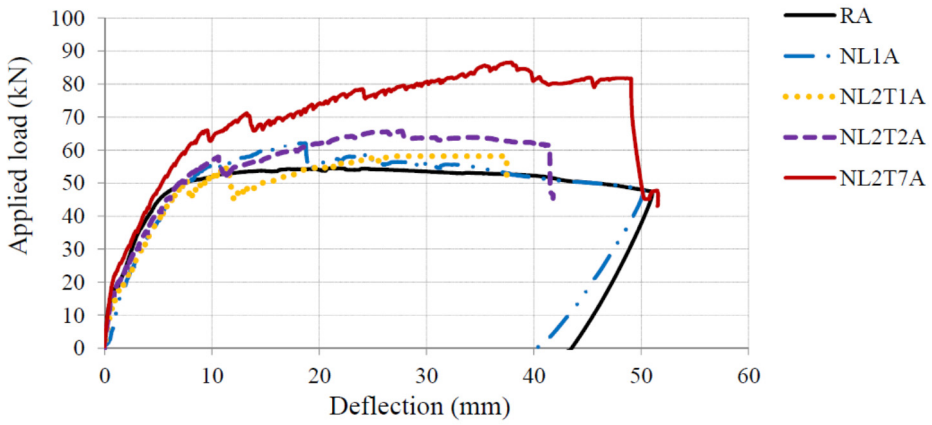

241

242 Figure 7. Load – displacement curves of rectangular beams (static)

243 The load – displacement curves of the modified-section beams are presented in Fig. 8. As
244 expected, the modified beams exhibited higher capacity than their counterpart in normal
245 rectangular section group. The increase of the capacity in Beams ML2T1A and ML2T2A was
246 23% and 34% compared to the reference beam. Interestingly, the capacity of Beam ML2T7A
247 increased 87% even though this beam used the same amount of materials and smaller cross-

sectional area as compared to Beam NL2T7A. It is recommended that the modified beams can be made by separately casting rectangular beams and curved segments before bonding them together by epoxy. The similar section modification method has been successfully used in previous studies [18-20]. At the maximum load, the FRP U-wraps of Beam NL2T7A did not rupture while the longitudinal FRP strip ruptured, which caused the failure. The curved soffit of this beam provides twofold advantages. It generated the normal stresses on the longitudinal FRP strip and increased the curvature of the bottom corner of the section, which eliminated stress concentration of the FRP U-wraps as shown in Fig. 1. As can be seen that r is a finite value in the case of the curved beam section so that the normal stress σ in FRP U-wraps provides confinement to the longitudinal FRP strip and then mitigates debonding failure of the longitudinal FRP strip (Eq. 1). On the other hand, r is infinite in the cases of the rectangular beams, thus the normal stress σ in the FRP U-wrap does not prevent debonding of the longitudinal FRP strips. Meanwhile, the FRP U-wrap restrains the longitudinal deformation of the longitudinal FRP sheets and thus increased the shear resistance at the interface but not the normal stress resistance.

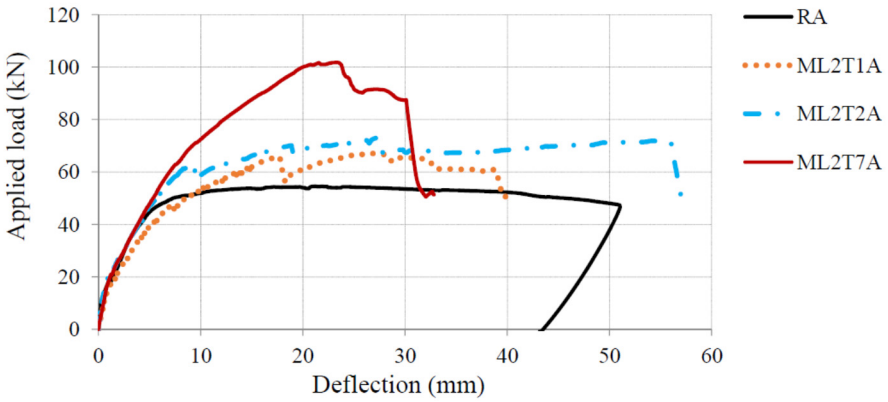

Figure 8. Load – displacement curves of modified-section beams (static)

4.3 Debonding strain of FRP

Debonding in FRP strengthened concrete structures takes place in regions of high stress concentrations, which are commonly associated with discontinuities and the presence of cracks. Propagation path of debonding initiates from stress concentrations is affected by the material properties and their interface rupture properties [21]. The FRP strain of Beam NL2T7A is shown in Fig. 9 to describe the debonding propagation and the debonding strain. It is noted that the locations of strain gauges are shown in Fig. 3. From Fig. 9, Strain Gauges L3 and L4 located near the midspan of the beam rose steadily at the early stage of loading. After 950 seconds, these strain gauges suddenly dropped while Strain Gauges L1 and L2 were activated at the same time. It means that debonding occurred and propagated to near the beam ends. Thus, the average value of Strain Gauges L3 and L4 is assumed as the debonding strain of this beam. In the meantime, the values of Strain Gauges TB1, TB2, TB3, and TB4 (25 mm above the beam soffit) were very small (less than 0.16%) and thus are not presented. Interestingly, these FRP U-wraps ruptured at the corners, implying the stress concentration at these positions was significantly high. The debonding strain of FRP of all the tested beams is summarized in Table 2.

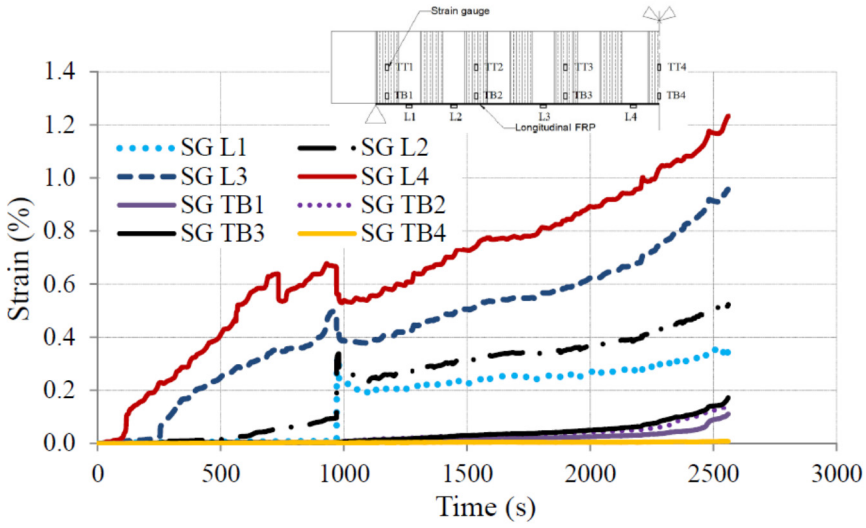

Figure 9. FRP strain of Beam NL2T7A

In order to demonstrate the effectiveness of the proposed beam modification, the FRP strains of Beams ML2T7A are shown in Fig. 10. At about 1300 seconds, Strain Gauges L3 and L4 reached the average value of 1.09% while Strain Gauges L2 and L1 suddenly jumped to about 0.4%. This phenomenon was caused by the propagation of FRP debonding from the midspan to the beam ends. In addition, some cracking sounds of the epoxy were heard at the same time. The beam then failed by rupture of the longitudinal FRP strip at midspan (Fig. 6e). Fig. 10 also shows that strain of the longitudinal FRP strip dropped while Strain Gauge TB4, which located on the FRP U-wrap at the midspan, suddenly jumped to a new value about 0.38%. It is obvious that the FRP strain of the proposed Beam MN2L7A was higher than the other rectangular beams and no stress concentration occurred. The debonding strain of FRP can be estimated based on bond strength models available in the literature as summarized in the study by Smith and Teng [22]. In order to estimate the debonding strain of FRP, the actual FRP thickness of the tested beams were measured at five different positions along the beams. The reported results in Table 2 are the average values of these measurements.

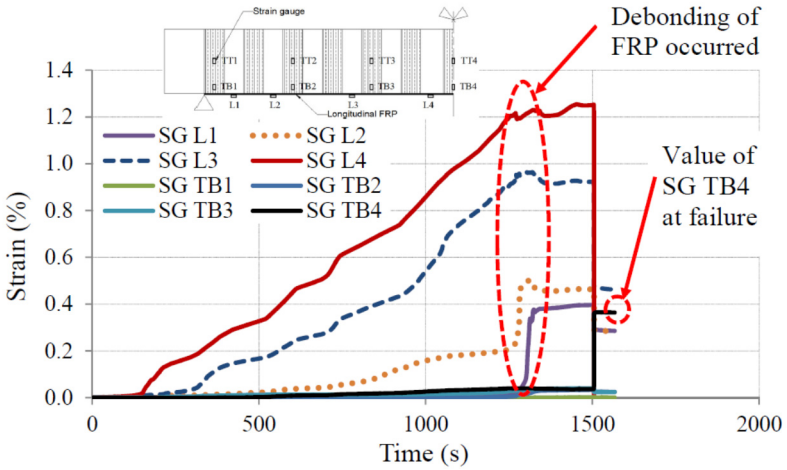

Figure 10. FRP strain of Beam ML2T7A

5 Experimental results of impact tests

5.1 Crack patterns and failure modes

Fig. 5 shows the crack patterns and failure modes of the tested beams. From this figure, it can be seen that the crack patterns of the tested beams under impact loads have shifted from vertical cracks in static tests to both inclined and vertical cracks. The vertical cracks distributed along the beams while the inclined cracks were observed at the impact zone surrounding the midspan. It means that failures of all beams tested under impact loads were governed by both the shear and flexure modes although the beams were designed with strong shear capacity. The number of vertical (flexural) and diagonal (shear) cracks of Beam RB are the same, indicating the dynamic shear and flexure capacities of this beam to resist impact loads are quite comparable. When the beam is strengthened with one longitudinal FRP layer (Beam NL1B), the static flexure capacity is thus increased. Beam NL1B still had some flexural cracks but the shear failure is more pronounced with wider shear cracks. Similar observations were observed in the cases of Beams NL2B, NL2T1B, and ML2T1B. Particularly, there were very few vertical cracks in Beam ML2T1B, indicating the effectiveness of applying FRP strips in enhancing the beam flexural capacity. As a result the shear failure governs the failure mode of this beam. As expected, Beams NL2T7B and ML2T7B exhibited less cracks than other tested beams with very small crack widths. As can be seen from Fig. 5 that the FRP U-wraps arrested the inclined cracks and prevented them from opening. These beams had only one vertical crack at the midspan under the impact zone as compared to the many shear cracks of the other beams without FRP U-wraps. This observation implies that the failure of these two beams was governed by the shear capacity.

All the impacted beams showed the local concrete crushing and scabbing damage at the impacted area. The maximum impact forces in these beams are about 500 kN corresponding to the contact area of 150 x 150 mm^2. The compressive stress of the concrete in the impact direction was about 22 MPa, which was smaller than the static compressive strength of the concrete (46 MPa). The compressive damage of the concrete was thus caused by the beam

326 global bending deformation. The photo of the compressive failure of the concrete underneath
327 the load adaptor supports this statement (Fig. 5). Beam RB failed with concrete crushing and
328 wide vertical and inclined cracks. These cracks were distributed in two third of the beam span
329 and no crack was found closer to the supports. From Fig. 5, stiffer beams exhibited less
330 number of cracks and the cracks distributed in a smaller area. Beams NL1B and NL2B failed
331 by debonding of the longitudinal FRP strip while Beams NL2T1B and ML2T1B failed by
332 debonding of the longitudinal FRP strip and rupture of the FRP U-wraps as shown in Figs.
333 11a-b. The longitudinal FRP strips did not rupture in these beams. In rectangular beams, the
334 FRP U-wraps were found to rupture at the corners owing to stress concentration (Fig. 11a).
335 However, the FRP U-wraps of modified-section beams did not rupture at the section corners
336 but failed at the intersection of the longitudinal and FRP U-wraps (Fig. 11b). Similar to Beam
337 NL2T7A, Beam NL2T7B failed owing to debonding of the longitudinal FRP strip and rupture
338 of the FRP U-wraps at the corners (Fig. 11c). Interestingly, Beam ML2T7B failed by
339 rupturing of the longitudinal FRP strip, similar to Beam ML2T7A. However, there was no
340 rupture of FRP U-wraps were found in Beam ML2T7A while the midspan FRP U-wrap of
341 Beam ML2T7B ruptured (Fig. 11d).

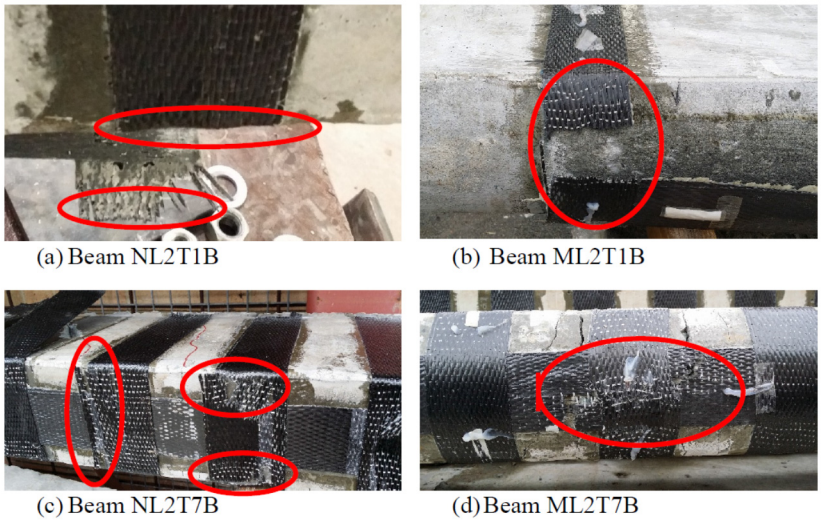

342
343 Figure 11. FRP rupture in impact tests

In addition, Fig. 12 shows the progressive failure of Beam NL1B. At the very early stage (1 millisecond, ms) after the impact, the first two shear cracks were observed, which initiated from the edges of the impact zone (the load adaptor) 45 degree toward the beam soffit. The two inclined cracks, which were resulted from the shear effect, formed a trapezium-shape concrete wedge below the impacted area. At 2 ms, there was one new vertical crack while the two existing cracks further opened as shown in Fig. 12c. A new short vertical crack appeared close to the beam soffit at 3 ms (Fig. 12d). At 4 ms, three new cracks were observed to initiate from the beam soffit upward. These new cracks were close to the vertical direction which is an indication of the flexure behavior dominance as shown in Fig. 12e. Subsequently, there was no new crack appeared in this region but the existing cracks further opened (Fig. 12f). Among these cracks, the two first inclined cracks were the longest and the widest so that they mainly dominated to the failure of the beam.

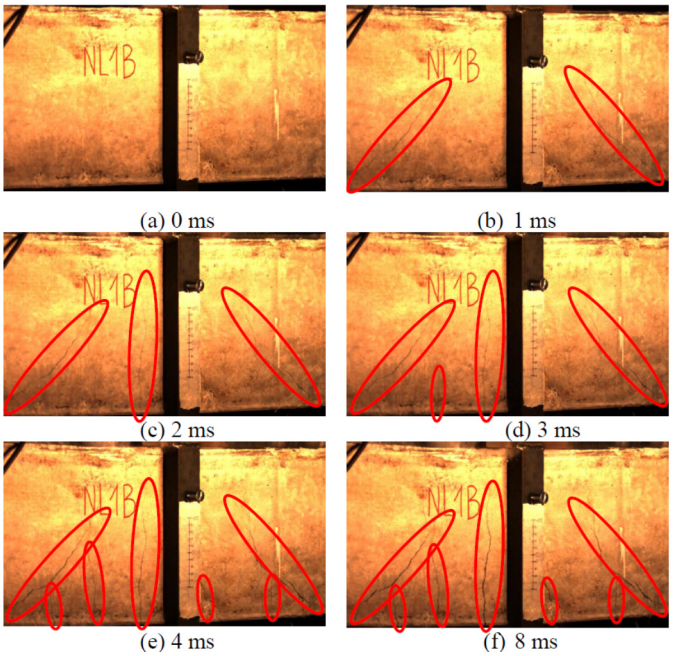

Figure 12. Progressive failure of Beam NL1B

5.2 Dynamic response

All impacted beams were tested by dropping a 203.5 kg projectile from the height of 2 m. The

theoretical impact velocity is 6.26 m/s, which was confirmed by actual impact velocity traced from the high speed camera images and presented in Table 3. This impact velocity may be close to the impact velocity in actual impact situations of dropping heavy objects on structures, rocks falling, and ship impacts on bridges. All beams failed after the first drop with debonding or/and rupture of FRP and large residual displacement. Fig. 13 shows the time histories of the impact force and reaction forces of all impacted beams during the first 50 millisecond (ms). The reaction force in the upward direction was assumed to be positive as in the case of static tests and vice versa. From this figure, it is observed that the responses of all beams have similar time history pattern. Firstly, the time history of the impact force exhibited the first peak with an isosceles triangle shape, high amplitude (about 450 kN) and short time duration (about 5 ms). Secondly, the triangular-shaped second peak was observed at 10 ms after the first peak. Subsequently, several local triangular-shaped peaks were found before the time history decreasing to zero at about 30 ms from the first peak.

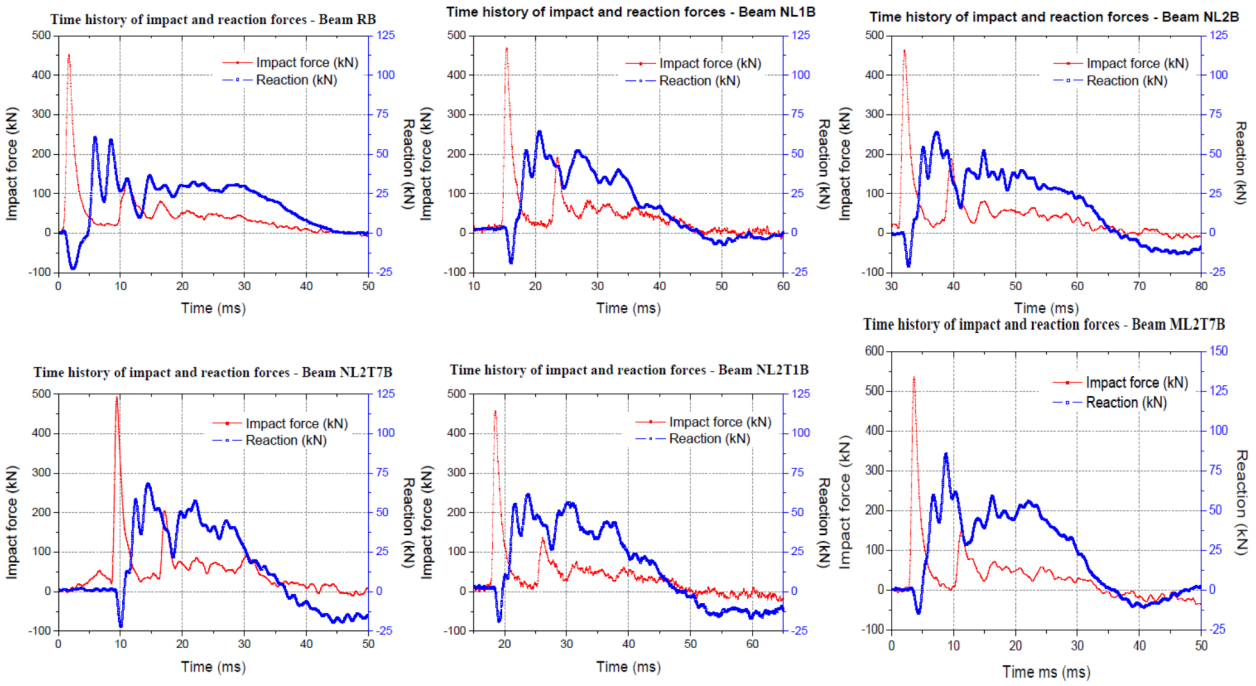

Figure 13. Time histories of impact and reaction forces

375 In the meantime, the time history of the reaction forces shows an interesting phenomenon. As
376 can be seen from Fig. 13, the negative reaction force was recorded before the positive reaction
377 force. It is worth noting that this phenomenon is also reported in previous studies [23, 24]. In
378 a numerical study about the behaviors of RC beams under high rate loading, Cotsovos [23]
379 found that a negative reaction was induced before the positive reaction was activated. In
380 addition, Kishi and Mikami [24] conducted an experimental study and also observed a similar
381 phenomenon that the negative reaction was induced before its positive counterpart. No
382 convincing explanation has been provided yet regarding this interesting observation. Attempt
383 to explain and understand this phenomenon is made here based on the theory of stress wave
384 propagation. It is well known that, upon impact on a solid surface, stress waves will be
385 generated and propagate in the solid, in which 67% of impact energy is converted to surface
386 Rayleigh wave, and Shear and P-wave account for the remaining 26% and 7% impact energy,
387 respectively [25]. P-wave and Shear wave propagate faster than Rayleigh wave and also
388 attenuate faster because of their relatively higher frequency contents. In the drop-weight tests,
389 stress waves are also generated in the beam and propagate from the impacted location at the
390 mid span towards the two ends. P-wave reaches the support first, followed by the Shear wave
391 and Rayleigh wave. Both the P-wave and Shear wave cause the beam vibrate in the horizontal
392 direction, where P-wave in the longitudinal direction while Shear wave in the transverse
393 direction. Vibrations in the horizontal directions do not generate vertical load, i.e. P-wave and
394 Shear wave arrival will not be measured by the load cell placed in the vertical direction. On
395 the other hand, Rayleigh wave causes beam vibrate in the vertical direction with elliptical
396 wave path along the beam surface. Arrival of Rayleigh wave will be measured by the vertical
397 load cell and results in negative force measurement of the upper load cell at the supports. This
398 is the likely reason for the observed negative reaction force measured in the tests at the initial

399 stage as shown in Fig. 13. More discussions to further support the above explanation will be
400 given in the next subsection.

401 In this study, the maximum negative reaction (lasted for about 5 ms) of about 20 kN was
402 recorded with an isosceles triangle shape. After the negative phase, the reaction force became
403 positive and reached its maximum value at approximately 60-86 kN. The time history of the
404 positive reaction force consisted of half-sine waves or triangular-shaped curves at the early
405 stage. After the main peak, the reaction force time history shows damped sinusoidal shapes
406 caused by vibration of the beam at a low frequency. The maximum value of the positive
407 reaction force was observed at the first or the second peaks. The positive reaction of Beam
408 RB reached the maximum value at 60 kN at the first peak while it obtained the maximum
409 value at the second peak in all the strengthened beams. Fig. 13 shows that the heavier
410 strengthened beams, the larger difference between the second and the first peak. For example,
411 the positive reaction force of Beam ML2T7B has the first peak 60 kN and the second peak 86
412 kN. The reason that the maximum reaction force in FRP strengthened RC beams appeared at
413 the second peak was because the deformation of the beam at the first loading peak activated
414 the FRP strips which increased the beam stiffness and loading capacities. The beams were
415 stiffer after the activation of the longitudinal FRP strips and they resulted in higher load
416 (reaction forces). It is evident from Fig. 13 that the reaction forces first appeared as negative
417 related to Rayleigh wave as explained above, they then increased to the maximum values in
418 the positive region owing to the global equilibrium of the beam under impact loadings before
419 reducing again to the negative region because of free vibrations of the beam. The first
420 maximum negative reaction forces were larger than their second counterparts associated with
421 the beam free vibrations.

The time histories of the displacement are shown in Fig. 14. It can be seen that all beams deflected from the original position to the maximum displacement and back to the residual deflection in about 35 ms. The maximum displacement and residual displacement of Beam RB were 52.3 mm and 41.6 mm, respectively. FRP strengthening significantly reduced the maximum displacement and the residual displacement of RC beams as compared to the reference beam (from 16% to 35%). The decrease percentage of the residual displacement is higher than that of the maximum displacement. Especially, strengthening Beam ML2T7B seems very successful since its maximum and residual displacements are greatly reduced by 35% and 44%, respectively. After reaching the first peak, these beams vibrated about 2 cycles before resting in the new balance positions.

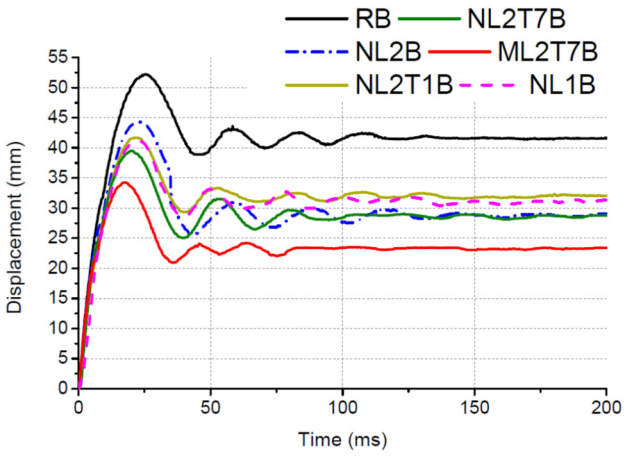

Figure 14. Time histories of displacement

5.3 Time delay of impact tests

As can be seen from Fig. 13, there was a time lag (time delay) between the impact force and the reaction forces. The time lag can be estimated from the difference between the activation time of the impact force and the reaction force. For further interpretation of the time lag, Fig. 15 provides a closer look at the time history of these forces. As shown in Fig. 15, the time lags vary from 0.7 ms to 0.9 ms. Without loss of generality, it is reasonable to assume that

the average time lag is 0.8 ms. The time lag is associated to the time required for stress waves to travel from the impact point to the supports. It is noted that the distance from the midspan to the supports is 0.95 m thus the stress wave velocity is estimated to be 1,188 m/s. This velocity is far different from the P-wave velocity of concrete which is about 3300 m/s. For concrete ($E \approx 25.10^9$ Nmm^{-2} and $\rho \approx 2400$ kgm^{-3}), the longitudinal stress wave velocity is c = $\sqrt{(E/\rho)}$. The time lag has been reported in previous studies [11, 23, 26-28]. However, no evident-based explanation has been provided in the literature. Banthia et al., [26] and Banthia et al., [27] reported in their experimental studies that the stress wave velocity estimated from the time lag was about 1,200 m/s. The authors explained that the reasons for this time lag include the discrete sampling interval and the possible initial softness of the beam supports. In order to clarify these possible causes, the present study ensures that the beam supports were properly tightened to a force of 80 kN and the sampling interval time was set to 0.02 ms, as compared to 0.2 ms in the study by Banthia et al., [26]. This sampling frequency should give sufficiently accurate recordings of the time lag of 0.8 ms. The similar estimated stress wave velocity in this study does not support the above reasons.

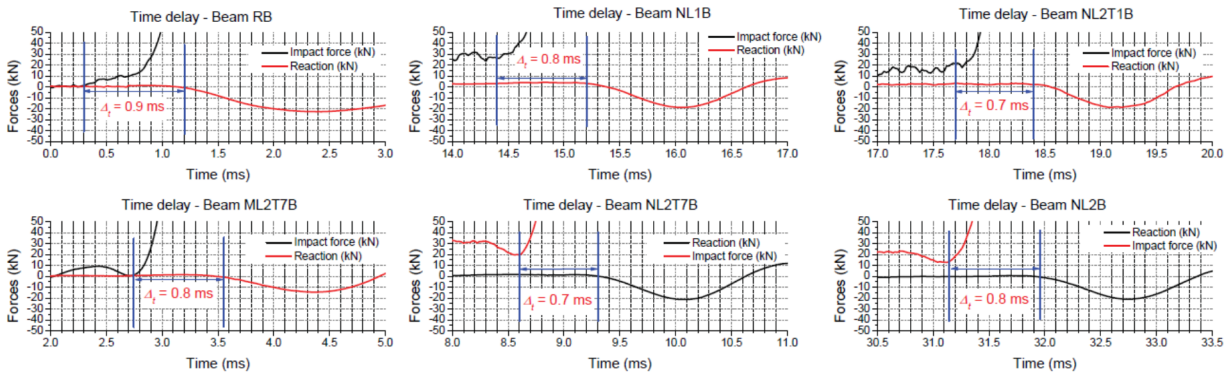

Figure 15. Time delay of impact tests

In addition, Cotsovos [23] conducted a numerical simulation and reported that the time lag was 0.5 ms for a distance of 1.35 m. The stress wave velocity in this case was 2,700 m/s which is closer to the longitudinal wave velocity in concrete. The author attributed the

460 discrepancy between the observed wave velocity and the actual wave velocity in concrete to
461 that the stress waves were unable to travel throughout the structural element length before loss
462 of load-carrying capacity. Isaac [28] reported in his PhD thesis the stress wave velocity was
463 about 750 m/s. The time lag in his tests was 0.7 ms corresponding to a distance of 0.5 m from
464 the midspan to the supports. Isaac suggested that the dominating propagating wave is not a
465 shear wave but a lower velocity wave.

466 In brief, there is a time lag between the impact force and the negative reaction forces, which
467 has been clarified by both experimental and numerical studies. The time lag can be explained
468 by the stress propagation theory. It is worth mentioning that two vertically oriented vibration
469 receivers should be used to measure the R wave velocity to obtain accurate measurements.
470 The time delay from two receivers is the travel time, which is a difference between the two
471 peaks of signal curves in time domain. In this study, the time delay between the peak impact
472 load and the peak negative reaction force was about 0.6 ms, smaller than 0.8 ms estimated
473 from wave arrivals, for a distance of 0.95 m. This is the time delay between the impact source
474 and the receiver not between two receivers. Using the time lag of 0.6 ms, the velocity of R
475 wave is thus about 1583 m/s, which is still smaller than the common value of the R wave
476 velocity in concrete, 2100 m/s to 2500 m/s [25]. However, it is noted that the impact force
477 was measured from a load cell placed on the top of the steel load adaptor on the beam.
478 Similarly, the load cells at the supports were not in direct contact with the beam either. There
479 exist a steel plate, a steel roller and a steel disk between the beam and load cell. As a result,
480 there exist a small time delay between the measured impact force and the force acting on the
481 beam, and a time delay between the stress wave on the beam and the measured reaction force
482 by the load cell at the supports. These contribute to the relatively large recorded time delay of
483 0.6 ms. Another reason for a small stress wave velocity is that the significant crushing
484 damage in concrete material at and near the impacting zone considerably reduces its Young's

485 modulus, which leads to smaller wave velocity. As can be seen in Fig. 13 that the impact
486 duration was about 5 ms while the first severe damage in concrete can be observed in the
487 specimens at 1 ms. It is thus evident that the concrete damage appeared at early stage and
488 during the traveling period of stress waves resulted in lower propagation velocity. In addition,
489 wave dispersion could also be a reason of the above phenomenon because the RC beam is not
490 an infinite half space, interaction between the coming waves and the reflected waves from
491 beam boundaries could change apparent wave propagation velocities.

492 In summary, Rayleigh wave propagation is used to explain the observed time lag between the
493 impact force and the recorded reaction force, and the initial negative reaction force in impact
494 tests. Further analyses and tests are necessary and will be carried out to confirm the
495 explanations.

496 ***5.4 Debonding strain of FRP***

497 The FRP strains of the impacted beams are shown in Fig. 15. The longitudinal FRP strips in
498 all impacted beams debonded from the concrete surface with exception of Beam ML2T7B.
499 Since impacted beams failed by FRP debonding, it is assumed that the maximum strain of the
500 longitudinal FRP strips is the debonding strain of FRP. In Beam NL1B strengthened with
501 only one longitudinal FRP strip, the debonding strain of FRP estimated from the average
502 strain of three Strain Gauges (SG) L2, L3, and L4 was 0.46%. The debonding strain of FRP in
503 Beam NL2T1B was 0.33%. The FRP strain in the FRP U-wraps was very small (<0.05%),
504 thus it is not presented in the figure. It is noted that SG L1 failed during the tests of the two
505 beams. Unfortunately, data of the FRP strains of Beams NL2B and ML2T1B was lost because
506 of a malfunction of the control computer.

507 It is interesting that although Beam NL2T7B failed by debonding of the longitudinal FRP
508 strip and fracture of the FRP U-wraps, the FRP strain on the FRP U-wraps was almost zero or

very small. The debonding FRP strain of Beam NL2T7B is 0.50%, which is an average of SGs L1, L2, and L4 since Strain Gauge L3 failed. On the other hand, Beam ML2T7B failed differently from all other beams so that more discussion is made on this beam. The longitudinal FRP strip of Beam ML2T7B debonded at vicinity of the midspan (SGs L2, L3 and L4) while it was still in the excellent bond condition at positions of SG L1. As can be seen from Fig. 16, SGs L2-4 had reached very high values while SG L1 was still very small (0.04%). It means that the modified-section beam together with FRP U-wraps prevented the longitudinal FRP strip from debonding. Especially, the longitudinal FRP strip ruptured at the midspan (SG L4) but unfortunately SG L4 failed after reaching the strain of 0.38%. The debonding strain of FRP (0.41%) is the average of SGs L2 and L3. In addition, the FRP U-wraps at the midspan had been activated as shown by the values of SG TB4. This strain gauge located near the beam soffit reached the maximum value at 0.21%. This FRP U-wrap then ruptured at middle of the beam soffit as shown in Fig. 11d. In addition, the longitudinal FRP strips reached their maximum values at about 2-2.5 ms which resulted in a strain rate of approximately 1.6 - 3 s^{-1}.

In brief, the debonding strain of FRP in impact tests was found to be smaller than its counterpart in the static tests. The impact stress wave with high amplitude may cause this reduction. It is noted that this study includes two identical sets of beams tested under static loads and impact loads, respectively. The first set of beams under static tests exhibited a pure flexure failure mode while the second set under impact loads failed in a combined mode (shear-flexure mode). The impact loads caused wider shear cracks which may result in high stress concentration of the longitudinal FRP strip. These two reasons possibly lead to the reduction of the FRP debonding strain in the impact tests.

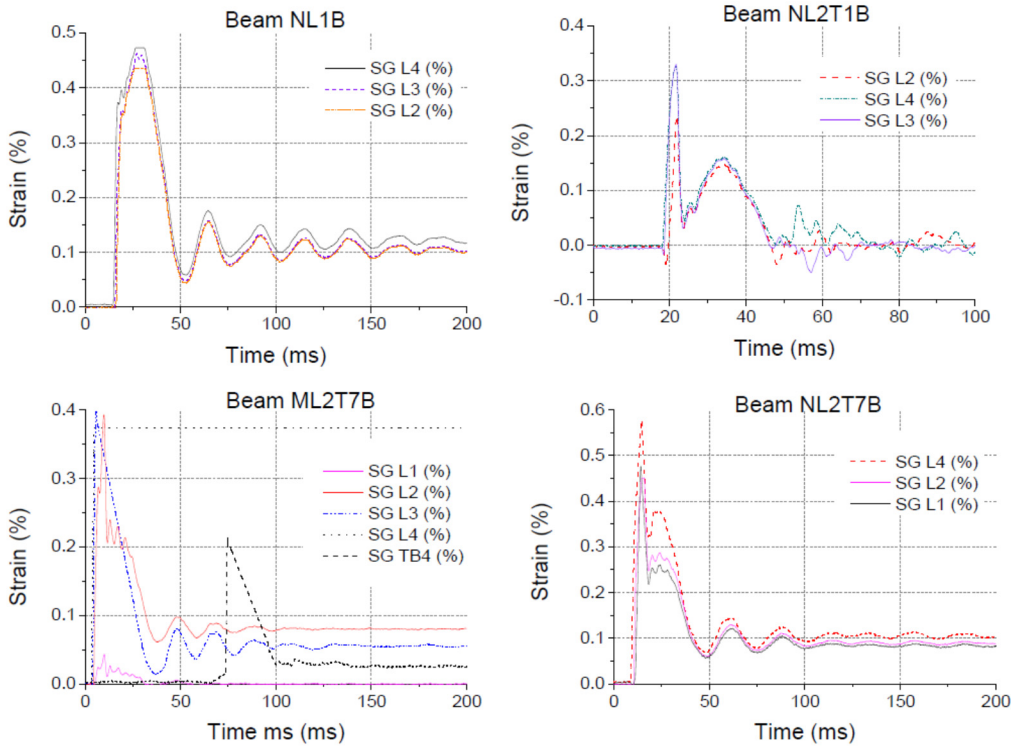

532

533 Figure 16. FRP strain of impacted beams

534 ***5.5 Shear dominance in impact tests***

535 From the experimental results above, it is interesting that all beams failed statically in the pure
536 flexure mode shifted to the shear-flexure mode in impact tests. As mentioned previously, the
537 shear dominance is more critical in impacted beams. This phenomenon can be explained as
538 follows: when a drop-weight impacts a beam and accelerates it, the beams is then balanced by
539 the participation of all force elements, such as impact force, reaction forces, and inertial forces
540 as presented in the study by Saatci and Vecchio [29]. However, since the impact force is
541 significantly higher than the reaction forces and there is a time delay between the impact force
542 and reaction forces as shown in Fig. 13, the force equilibrium is maintained because of the
543 inertial forces during the action of impact force.

544 The acceleration of the beam causes inertial forces as presented in previous studies. Banthia et
545 al., [30] experimentally proposed the distribution of the inertial forces along the beam at

546 which the distribution is linear in the case of plain concrete and sinusoidal in the case of RC
547 concrete. There is a consensus that the impact force is resisted by the inertial forces at very
548 early moment of an impact event [23, 29, 31]. Experimental results from this study also
549 confirm this assumption since no reaction forces or very small value of the negative reaction
550 force was observed during the action of the impact force (Fig. 13). The free body diagram for
551 dynamic equilibrium of the impacted beams at the very early moment is presented in Fig. 17.
552 For simplicity, the distribution of the inertial forces along the beam is assumed to be linear.
553 The resulting moment of the beams at the maximum impact force can be estimated in the
554 following two steps: (1) since reaction forces are zero and the sum of the initial force is then
555 equal to the maximum impact force, the values of distributed initial force can be computed;
556 (2) considering a half of the beams and taking moment about the midspan section results in
557 Equation 3.

558
$$M = \frac{P}{L\left(1-\frac{4a^2}{L^2}\right)}\left(\frac{L^2}{12}-a^2-\frac{4a^3}{3L}\right) \tag{3}$$

559 where M is the resulting moment, P is the impact force, L is the beam span, and a is the
560 overhang length.

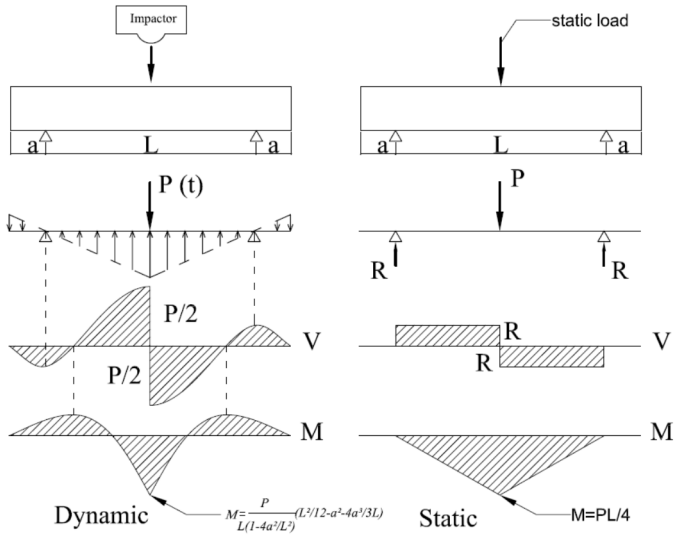

561

562 Figure 17. Distribution of forces and resulting moment and shear diagrams

563 The impact force can be estimated as presented in the study by Pham and Hao [32].
564 Considering the peak impact force P and performing static equilibrium analysis, the largest
565 shear force equals to $P/2$ in the both cases as shown in Fig. 17, but the peak dynamic bending
566 moment is equal to $PL/12$ if overhang a is assumed to be zero, which is three times smaller
567 than that obtained in static case. Therefore a beam that experiences flexural damage under
568 static loading might suffer shear damage under impact load. In addition, the shear force in the
569 beam is equal to the reaction in the static cases (about <50 kN) while the shear force at the
570 midspan of impacted beams is equal to half of the impact forces (approximately 250 kN). The
571 shear force in the impacted beam is thus five times higher than that in the static cases. As a
572 result, the shear failure became more critical in the impacted beams. It is recommended that
573 the shear failure mode should be carefully considered in such cases.

574 **6 Conclusions**

575 This study investigates the behavior of RC concrete beams strengthened with FRP under both
576 quasi-static and impact loads. The proposed beam modifications have been demonstrated
577 successful in increasing the beam capacities in both loading conditions. The findings in this
578 study are summarized as follows:

579 1. The proposed beam section modification delays the debonding of FRP and reduces the
580 stress concentration at the corners. They significantly increased the beam capacities
581 even though the same amount of materials are used as compared to its rectangular
582 counterparts.

583 2. Using FRP U-wraps is highly recommended to maximize the capability of longitudinal
584 FRP strips.

3. RC beams failed in the flexure mode in static tests may fail by shear-flexure mode under impact loads.

4. The impact force and inertial forces at the very early moment of an impact event should be used to design the impact resistance.

5. Locally strengthening RC beams in shear at the expected impacting region is crucial to prevent the shear failure.

6. Impact loads might cause premature debonding of FRP so that anchor system should be used to strengthening RC beams against impact loads.

Finally, the experimental results showed that FRP can be used to strengthen RC beams against impact loads. However, debonding of FRP and shear dominance in impact tests should be carefully taken into account. Analyses of the observed initial negative reaction forces and time delay between the impact loads and reaction forces have also been carried out. Possible explanations of these phenomena in impact testing have been provided.

References

[1] Nguyen-Minh L, Rovňák M. Punching Shear Resistance of Interior GFRP Reinforced Slab-Column Connections. Journal of Composites for Construction. 2013;17:2-13.
[2] Mutalib AA, Hao H. Numerical Analysis of FRP-Composite-Strengthened RC Panels with Anchorages against Blast Loads. Journal of Performance of Constructed Facilities. 2011;25:360-72.
[3] White T, Soudki K, Erki M. Response of RC Beams Strengthened with CFRP Laminates and Subjected to a High Rate of Loading. Journal of Composites for Construction. 2001;5:153-62.
[4] Tang T, Saadatmanesh H. Analytical and experimental studies of fiber-reinforced polymer-strengthened concrete beams under impact loading. ACI Structural Journal. 2005;102:139-49.
[5] Erki M, Meier U. Impact loading of concrete beams externally strengthened with CFRP laminates. Journal of Composites for Construction. 1999;3:117-24.
[6] Tang T, Saadatmanesh H. Behavior of Concrete Beams Strengthened with Fiber-Reinforced Polymer Laminates under Impact Loading. Journal of Composites for Construction. 2003;7:209-18.

615 [7] Pham TM, Hao H. Impact Behavior of FRP-Strengthened RC Beams without Stirrups.
616 Journal of Composites for Construction. 2016;DOI: 10.1061/(ASCE)CC.1943-
617 5614.0000671:04016011.
618 [8] ACI 440.2R-08. Guide for the Design and Construction of Externally Bonded FRP
619 Systems for Strengthening Concrete Structures. 4402R-08. Farmington Hills, MI: American
620 Concrete Institute; 2008.
621 [9] Smith ST, Teng JG. FRP-strengthened RC beams. I: review of debonding strength models.
622 Engineering Structures. 2002;24:385-95.
623 [10] Hamed E, Rabinovitch O. Dynamic Behavior of Reinforced Concrete Beams
624 Strengthened with Composite Materials. Journal of Composites for Construction. 2005;9:429-
625 40.
626 [11] Fujikake K, Li B, Soeun S. Impact response of reinforced concrete beam and its
627 analytical evaluation. Journal of Structural Engineering. 2009;135:938-50.
628 [12] Pham TM, Hadi MNS. Stress Prediction Model for FRP Confined Rectangular Concrete
629 Columns with Rounded Corners. Journal of Composites for Construction. 2014;18:04013019.
630 [13] MacGregor JG. Reinforced concrete: mechanics and design. Upper Saddle River, N.J:
631 Prentice Hall, 2005.
632 [14] West System n.d. Epoxy resins and hardeners - Physical properties. 2015.
633 [15] Pham TM, Hadi MNS, Tran TM. Maximum usable strain of FRP-confined concrete.
634 Construction and Building Materials. 2015;83:119-27.
635 [16] Pham TM, Hadi MNS, Youssef J. Optimized FRP Wrapping Schemes for Circular
636 Concrete Columns. Journal of Composites for Construction. 2015;19:04015015.
637 [17] ASTM D3039. Standard Test Method for Tensile Properties of Polymer Matrix
638 Composite Materials. D3039:2008. West Conshohocken, PA2008.
639 [18] Pham TM, Doan LV, Hadi MNS. Strengthening square reinforced concrete columns by
640 circularisation and FRP confinement. Construction and Building Materials. 2013;49:490-9.
641 [19] Hadi MNS, Pham TM, Lei X. New Method of Strengthening Reinforced Concrete
642 Square Columns by Circularizing and Wrapping with Fiber-Reinforced Polymer or Steel
643 Straps. Journal of Composites for Construction. 2013;17:229-38.
644 [20] Priestley MJN, Seible F. Design of seismic retrofit measures for concrete and masonry
645 structures. Construction and Building Materials. 1995;9:365-77.
646 [21] Buyukozturk O, Gunes O, Karaca E. Progress on understanding debonding problems in
647 reinforced concrete and steel members strengthened using FRP composites. Construction and
648 Building Materials. 2004;18:9-19.
649 [22] Smith ST, Teng J. FRP-strengthened RC beams. II: assessment of debonding strength
650 models. Engineering Structures. 2002;24:397-417.
651 [23] Cotsovos DM. A simplified approach for assessing the load-carrying capacity of
652 reinforced concrete beams under concentrated load applied at high rates. International Journal
653 of Impact Engineering. 2010;37:907-17.
654 [24] Kishi N, Mikami H. Empirical formulas for designing reinforced concrete beams under
655 impact loading. ACI Structural Journal. 2012;109:509-19.
656 [25] Rhazi J, Hassaim M, Ballivy G, Hunaidi O. Effects of concrete non-homogeneity on
657 Rayleigh waves dispersion. Magazine of Concrete Research. 2002;54:193-201.
658 [26] Banthia NP, Mindess S, Bentur A. Impact behaviour of concrete beams. Materials and
659 Structures. 1987;20:293-302.
660 [27] Banthia N, Mindess S, Bentur A. Energy balance in instrumented impact tests on plain
661 concrete beams. Fracture of Concrete and Rock: Springer; 1989. p. 26-36.
662 [28] Isaac PM. Effects of Extreme Impulsive Loads on RC Structures with a view to
663 Strengthening [Dissertation]: University of Bath, 2014.

664 [29] Saatci S, Vecchio FJ. Effects of shear mechanisms on impact behavior of reinforced
665 concrete beams. ACI Structural Journal. 2009;106:78-86.
666 [30] Banthia N, Mindess S, Bentur A, Pigeon M. Impact testing of concrete using a drop-
667 weight impact machine. Experimental Mechanics. 1989;29:63-9.
668 [31] Cotsovos D, Stathopoulos N, Zeris C. Behavior of RC beams subjected to high rates of
669 concentrated loading. Journal of Structural Engineering. 2008;134:1839-51.
670 [32] Pham TM, Hao H. Prediction of the Impact Force on RC Beams from a Drop Weight.
671 Advances in Structural Engineering. 2016;DOI: 10.1177/1369433216649384.
672

673 **List of Figures**

691 **List of Tables**

695 Table 1. Test matrix

ID	Section	Longitudinal FRP (layers)	Transverse FRP (strips)	Static shear capacity (kN)	Static flexural capacity (kNm)
R-A	Rectangular	-	-	93	21
R-B	Rectangular	-	-	93	21
N-L1-A	Rectangular	1	-	93	23
N-L1-B	Rectangular	1	-	93	23
N-L2-B	Rectangular	2	-	93	25
N-L2T1-A	Rectangular	2	1	93	25
N-L2T1-B	Rectangular	2	1	93	25
N-L2T7-A	Rectangular	2	7	123	-
N-L2T7-B	Rectangular	2	7	123	-
M-L2T1-A	Modified	2	1	93	25
M-L2T7-A	Modified	2	7	93	25
M-L2T1-B	Modified	2	1	123	-
M-L2T7-B	Modified	2	7	123	-

696 - Not applicable

697 Table 2. Experimental results of static tests

Beams	Maximum load	Maximum Displacement	Debonding strain	Actual thickness of FRP	*Load increase
	kN	mm	%	mm	%
RA	54.5	51.0	-	-	-
NL1A	62.1	50.2	0.59	1.1	14.0
NL2T1A	58.2	37.5	0.41	1.8	6.8
NL2T2A	65.2	41.2	0.56	1.7	19.6
NL2T7A	86.6	51.6	0.60	2.1	58.9
ML2T1A	67.1	38.9	0.41	1.8	23.1
ML2T2A	73.1	56.1	0.67	1.9	34.1
ML2T7A	101.8	30.2	1.09	2.1	86.8

698 - Not applicable
699 * as compared to the corresponding value of reference beam

700 Table 3. Experimental results of impact tests

Beams	Impact force	Impact velocity	Positive reaction force	Negative reaction force	Debonding strain	Maximum displacement	Residual displacement	Impact force increase	Reaction force increase
	kN	m/s	kN	kN	%	mm	mm	%	%
RB	453	6.3	60	-23	-	52.3	41.6	-	-
NL1B	470	6.3	62	-19	0.46	41.1	31.2	3.8	3.3
NL2B	464	6.1	64	-21	-	44.2	28.7	2.4	6.7
NL2T1B	460	6.3	65	-20	0.33	41.7	31.7	1.5	8.3
NL2T7B	492	6.2	68	-23	0.50	39.5	29.8	8.6	13.3
ML2T1B*	-	6.2	-	-	-	43.8	33.7	-	-
ML2T7B	536	6.3	86	-15	0.41	34.2	23.4	18.3	43.3

701 - Not applicable
702 *Test data of Beam ML2T1B were lost because of malfunction of the control computer. The displacement was calculated from the high speed
703 camera.